Probing Catalyst Speciation in Pd-MPAAM-Catalyzed Enantioselective C(sp^3)-H Arylation: Catalyst Improvement via Destabilization of Off-Cycle Species

Wei Hao,[1] Katherine L. Bay,[2§] Caleb F. Harris,[3] Daniel S. King,[2] Ilia A. Guzei,[3] Zhe Zhuang,[1] R. Erik Plata,[1†] David E. Hill,[1‡] K. N. Houk,[2*] John F. Berry,[3*] Jin-Quan Yu,[1*] and Donna G. Blackmond[1*]

[1]Department of Chemistry, Scripps Research, La Jolla, CA 92037 USA; [2]Department of Chemistry and Biochemistry, University of California Los Angeles, CA 90095 USA; [3]Department of Chemistry, University of Wisconsin, Madison, WI 53706 USA

ABSTRACT: Chiral monoprotected aminoethyl amine (MPAAM) ligands were recently reported to facilitate enantioselective Pd-catalyzed arylation of strong cyclopropane C(sp^3)–H bonds. Herein, we describe detailed experimental and theoretical investigations into the influence of MPAAM ligands, **L1** and **L2**, as well as monoprotected aminoethyl thioether (MPAThio) ligand, **L3**, on reaction kinetics, product enantioselectivity, and turnover number. We show an unusual negative nonlinear effect in ligand enantiopurity on rate and *ee* that has not been shown previously in CH activation reactions, along with a negative dependence of ligand concentration on reaction rate. NMR titrations, kinetic modeling, crystal structures, and DFT calculations implicate concentration-dependent formation of stable, off-cycle, homoleptic Pd(L)$_2$ species in the presence of **L1** or **L3**. However, in the **L2** system, results suggest that only the catalytically active, mono-substituted [Pd(L)(OAc)] species is formed, regardless of ligand concentration, demonstrating the subtle influence of ligand structure on reaction kinetics and mechanism. The impact of these mechanistic findings on ligand design is demonstrated by the results using a new ligand in the MPAAM family, **L2**, which exhibits higher reaction rates.

Keywords: C-H activation, kinetics, nonlinear effects, enantioselective catalysis, Pd catalysis, reaction mechanism

INTRODUCTION

Applications of chiral, small molecule ligand architectures in new catalyst design have led to significant advances in the field of site-specific and enantioselective C–H bond functionalization.[1] Amongst the ligands currently available, those utilizing the privileged AcNH motif have witnessed particular success.[2-5] Examples of such ligands introduced by the Yu group shown in Scheme 1 include: MonoProtected Amino Acids (MPAA),[2] Mono-N-Protected Aminomethyl Oxazoline (MPAO),[3] Acetyl-Protected Aminoethyl Quinolines (APAQ),[4] and MonoProtected Aminoethyl AMine (MPAAM)[5] and its sulfur derived analog MonoProtected Aminoethyl Thioether (MPAThio).[6] This suite of ligands has enabled the functionalization of a wide variety of difficult C–H bonds, including the strong C(sp^3)–H bonds of cyclopropane. Systems employing this motif have been studied extensively by a number of other research groups.[7]

Scheme 1. Privileged Ligands in C-H Functionalization.

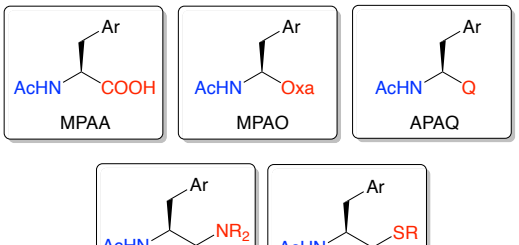

While catalysts that employ these families of ligands have been efficacious in obtaining desired selectivity, much less is understood about the coordination mode of the ligands, catalyst speciation in solution, or the overall reaction mechanism. For labile, catalytically active Pd(II) complexes, catalyst speciation can be particularly problematic. Although the formation of off-cycle, homoleptic Pd(**L**)$_2$ species with mono-dentate pyridine ligand in C-H activation reactions was reported previously,[8] related phenomenon with bidentate ligands and their impact on enantioselection have not been investigated so far. Similar supporting ligands can give rise to mono-Pd as well as higher order species,[2-7] and observable species may not necessarily be catalytically active (i.e., they can be off-cycle intermediates). It is therefore not necessarily obvious given a particular ligand structure what the key on- or off-cycle species may be. It has been shown that a nonlinear response of reaction product *ee* to the *ee* of the chiral ligands employed can be diagnostic for presence of interme-

diate species with multiple ligands.[4b,9-11] Such indirect mechanistic data are powerful in probing complex systems such as the above-mentioned Pd-catalyzed C–H functionalization reactions, where the applicability of other analytical tools may be limited.

In this study, we highlight an unusual system in which structural predictions from the observation of nonlinear effects on *ee* and rate are fully substantiated by direct crystallographic and spectroscopic characterization and computational data on the isolated Pd complexes. We report here the first structural characterization of mononuclear Pd^{II} complexes bearing the AcNH functionalized MPAAM (**L1**, **L2**) and MPAThio (**L3**) ligands shown in Scheme 2. Furthermore, we describe detailed experimental, computational, and kinetic analyses that examine the nature of the active catalyst and the origins of enantioselectivity for functionalization of extraordinarily strong cyclopropyl C–H bonds.

Scheme 2. Reaction Conditions Employed in Mechanistic Investigations.

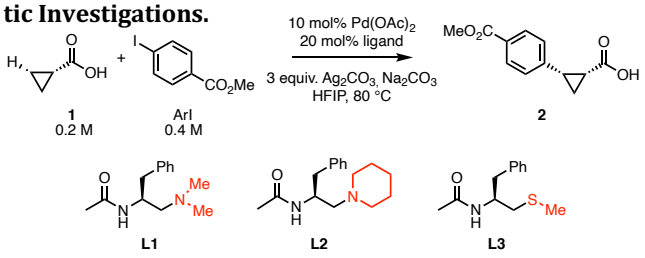

RESULTS AND DISCUSSION

The previously reported *N,N*-dimethyl substituted **L1** was employed with Pd in the reaction shown in Scheme 2. Our investigation revealed that this ligand system exhibits an unusual *negative* nonlinear effect on enantioselectivity (Figure 1).[14] Similar behavior was exhibited by the analogous thio ligand **L3**. Interestingly, however, subtle differences in the steric environment of the tertiary amine (-NR_2) for **L2** provided a system that shows linear behavior between catalyst and reaction product *ee*. Figure 1 also shows that for reactions with **L1**, employing racemic ligand resulted in an unusual *increase* in reaction rate compared to enantiopure ligand, while systems with **L2** gave identical rates for racemic and enantiopure ligand.

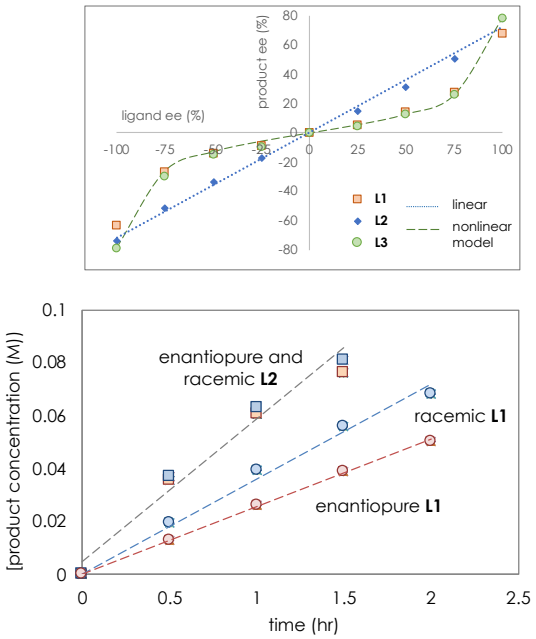

Figure 1. Top: Relationship between product **3** *ee* and ligand *ee* for reactions using ligands **L1**, **L2**, and **L3**. Bottom: kinetic profiles for reactions using racemic and enantiopure ligands **L1** and **L2**. $[\mathbf{1}]_0$ = 0.2 M; $[\mathbf{2}]_0$ = 0.4 M; $[Pd]_0$ = 0.02 M and Pd:L = 1:4. Symbols represent experimental data; dotted line in top plot shows the linear relationship; dashed line in top plot shows the model prediction of the negative nonlinear effect (see discussion in text).[14]

Since the observation of a nonlinear effect in asymmetric catalysis implies the presence of species with multiple ligands, either on or off the catalytic cycle,[9-11] we sought evidence through ligand binding titration experiments for the formation of higher-order PdL_x (x > 1) complexes. The interaction of free **L1** and $Pd(OAc)_2$ was initially evaluated by ^{1}H-NMR spectroscopy, however, rapid line broadening and the overlapping of signals convoluted the interpretation of the data. We employed ^{19}F NMR spectroscopy using enantiopure fluorine-labeled derivatives of the ligands, **L1-F** and **L2-F** to probe the interaction between $Pd(OAc)_2$ and the ligands (Figure 2). Addition of base to the Pd-**L1-F** or Pd-**L2-F** system resulted in little change to the ^{19}F or ^{1}H NMR spectra.[14] As shown in Figure 2a, the spectra for the **L1-F** system show two peaks present in the reaction mixtures. At substoichiometric L:Pd ratios, the signal for free ligand at -117.4 ppm is shifted to -117.2 ppm but gradually moves back towards that of the free ligand as the concentration of **L1-F** increases. The second peak at -118.4 ppm also appears at a low L:Pd ratio yet experiences less of a change in chemical shift with respect to increased ligand concentrations. DOSY measurements confirmed that the species represented by the two peaks exhibit different diffusion coefficients.[14] HRMS analysis of the solution of **L1-F** and $Pd(OAc)_2$ identified a bis-ligated Pd species $Pd(L1\text{-}F)_2$ [M+H] ($C_{26}H_{36}F_2N_4O_2{}^{102}Pd$: mass 577.1941 (calculated), 577.1953 (found)).

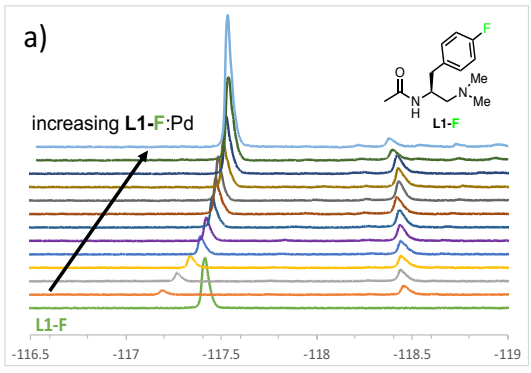

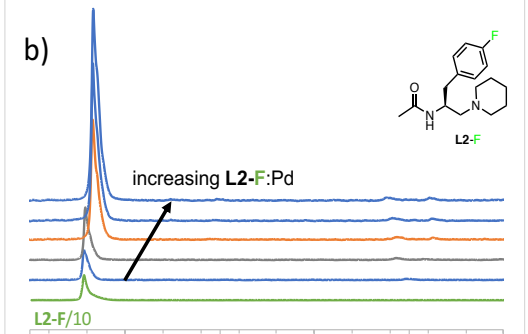

Figure 2. ^{19}F-NMR spectra of interactions between Pd and fluorinated versions of **L1** and **L2**. [Pd] = 0.06 M. Stock solutions of ligand and $Pd(OAc)_2$ in HFIP were added to the NMR tube with a trifluoroethylene coaxial insert. Spectra were recorded after 10 min at 55 °C.[14] Pure ligand in the absence of Pd shown as the lowest spectrum in green (**L1**-F = 0.06 M; **L2-F** = 0.3 M, scaled by a factor of 10). Pd:L ratios: a) 1:0.5, 1:0.67, 1:0.83, 1:1, 1:1.17, 1:1.33, 1:1.5, 1:1.67, 1:1.83 1:2, 1:3, 1:4; b)1:1, 1:2, 1:3, 1:4, 1:5.

We confirmed that the ^{19}F-NMR spectra in Figure 2 showing two peaks for the **L1-F** system and a single peak for the **L2-F** system are identical under reaction conditions.[14] Since addition of free **L1-F** to $Pd(OAc)_2$ gives a dynamic system with more than one species present in solution, we developed a targeted synthetic approach that has allowed us to characterize several important Pd species, including those that may be disfavored under the reaction conditions described in Scheme 2. As outlined in eq 1, the ligands were first deprotonated with either potassium or lithium bis(trimetylsilyl)amide and subsequently transferred to a solution of $Pd(OAc)_2$ or $Pd(MeCN)_2Cl_2$ in a THF/Et_2O mixture. In each case, the corresponding Pd(**L**)$_2$ complex precipitated as a light yellow solid. Single crystals suitable for X-ray diffraction were prepared by solvent diffusion of pentane into concentrated dichloromethane solutions of Pd(**L**)$_2$ (Figure 3). These complexes represent the first structural characterizations of Pd complexes with either MPAAM or MPAThio family ligands. In these materials, the deprotonated amide coordinates to Pd through the nitrogen as an X-type ligand, while the tertiary amine in **L1,** and thioether in **L3,** acts as an L-type donor, forming a 5-membered palladacycle.

$$2\,HL \xrightarrow[\text{Pd}X_2\ (X = OAc,\ Cl)]{2\text{ eq. KHMDS/LiHMDS}} PdL_2 \qquad (1)$$

This synthetic method appears to be quite general. In addition to the homoleptic Pd(**L**$_R$)$_2$ compounds, [(*R,R*)-Pd(**L1**)$_2$] and [(*R,R*)-Pd(**L3**)$_2$], we have also been able to prepare the heterochiral [(*R,S*)-Pd(**L3**)$_2$] shown in Figure 3. The latter complex was prepared by sequentially treating $Pd(OAc)_2$ with one equivalent of (*R*)-K(**L3**) followed by one equivalent of (*S*)-K(**L3**).

The crystal structures of the three complexes all show Pd(II) in a slightly distorted square-planar coordination environment. The two ligands are coordinated in a bidentate fashion through the terminal amino (L1 and L2) or thio group (L3), and the N atom of the deprotonated amide. The resulting five-membered palladacycles form N-Pd-heteroatom bond angles ranging from 76.2(6)° to 84.6(3)°. The Pd-N bond distances between the metal and the deprotonated amide ranged from 2.024(5) to 2.059(7) Å, similar to other complexes in which an amide was part of the five-membered palladacycle.[15] In the model for complex [(R,R)-Pd(L1)2], Li and Cl atoms that formed as a by-product of the synthetic route were found intercalated within the structure. Tables of bond lengths and angles are shown in the Supporting Information.

DFT structures were calculated for ligand systems **L1** and **L3** as shown in Figures 4 and 5, respectively.[14] To ensure that the relative energies were always compared to systems with the same number of atoms, the energies of a Pd monomer, such as [R-Pd(L1)(OAc)], plus one protonated L1 ligand was compared to the energies Pd dimer, such as [(R,R)-Pd(L1)2] plus one acetic acid molecule. We have shown in previous papers that acetate-bridged Pd dimers are much higher in energy than acetate-bridged Pd trimers.[16] We used the Pd acetate trimers as the reference and found that the formation of the bis-ligated structures is favorable.[14] The most stable species for ligand L1 is the homoleptic *trans*-[(*R,R*)-Pd(**L1**)$_2$], as characterized crystallographically, which lies 1.3 kcal/mol lower than it's *cis*-isomer and 2.6 kcal/mol below the mono-ligated [(*R*)-Pd(**L1**)(OAc)] (Figure 4). This assignment is in good agreement with the crystal structure shown in Figure 3a.

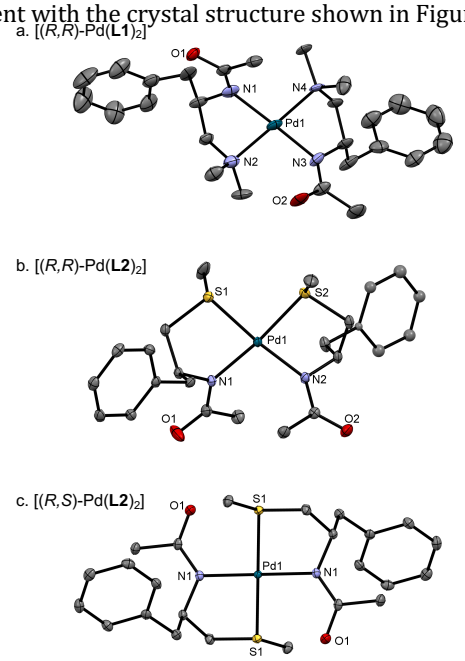

Figure 3. Crystal structures of (a) (*R,R*)-Pd(**L1**)$_2$, (b) (*R,R*)-Pd(**L3**)$_2$, and (c) (*R,S*)-Pd(**L3**)$_2$. Thermal ellipsoids are drawn at the 50% probability level with hydrogen atoms and outer sphere LiCl atoms omitted for clarity. For (b), one of the phenyl rings was disordered and stable refinement required isotropic modeling of the thermal parameters.

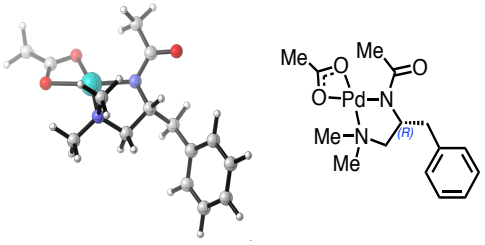

[*R*-Pd(L1)(OAc)]: ΔΔG = 2.6 kcal mol^{-1}

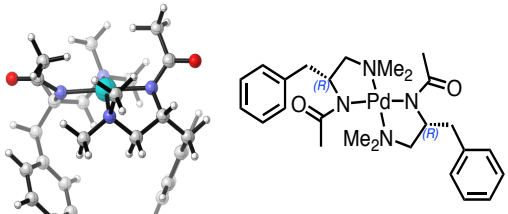

Figure 4. Relative stabilities of lowest energy conformers of species formed from $Pd(OAc)_2$ and **L1**. [*R*-Pd(**L1**)(OAc)] (top), [(*R,R*)-Pd(**L1**)$_2$] (middle), and [(*R,S*)-Pd(**L1**)] (bottom). SMD (Generic, ε=16.7)/M06/6-311+G(d,p)//B3LYP/6-31G(d).

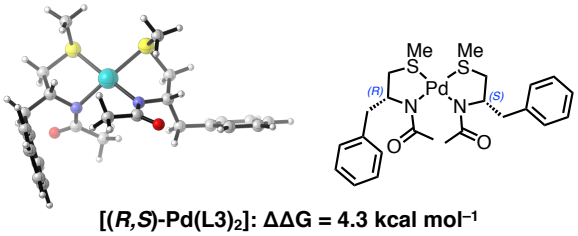

[(*R,S*)-Pd(L3)$_2$]: ΔΔG = 4.3 kcal mol^{-1}

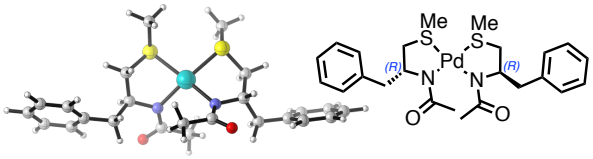

[(*R,R*)-Pd(L3)$_2$]: ΔΔG = 0.0 kcal mol^{-1}

Figure 5. Relative stabilities of lowest energy conformers of species formed from $Pd(OAc)_2$ and **L3**. [(*R,S*)-Pd(**L3**)$_2$] (top), [(*R,R*)-Pd(**L3**)$_2$] (bottom). SMD (Generic,eps=16.7)/M06/6-311+G(d,p)// B3LYP/6-31G(d).

The next lowest energy configuration, heterochiral *cis*-[(*R,S*)-Pd(**L1**)$_2$], lies 4.8 kcal/mol above *trans*-[(*R,R*)-Pd(**L1**)$_2$]. Dimeric (Pd**L**)$_2$ complexes are significantly (> 20 kcal/mol, see Supporting Information) less stable than the monomeric Pd(**L**)$_2$ complexes. Thus, the homoleptic *trans*-[(*R,R*)-Pd(**L1**)$_2$] and the mono-ligated species likely comprise most of the [Pd] population for the **L1** system. The mono-ligated [(*R*)-Pd(**L1**)(OAc)] species retains an acetate ligand and presumably represents the active entry into the catalytic cycle.

As shown in Figure 5, calculations with ligand **L3** also implicate a homoleptic species, *cis*-[(*S,S*)-Pd(**L3**)$_2$], as the most stable, lower in energy by 4.3 kcal/mol compared to the heterochiral species, *cis*-[(*S,R*)-Pd(**L3**)$_2$]. As with **L1**, the population of [Pd] species for **L3** is likely a mixture of monosubstituted [(*S*)-Pd(**L3**)(OAc)] and homochiral *cis*-[(*S,S*)-Pd(**L3**)$_2$]. In contrast to **L1**, both *bis*-ligated **L3** complexes prefer the *cis* conformation. The crystal structure of the homochiral *cis*-[(*R,R*)-Pd(**L3**)$_2$] complex shown in Figure 3b supports these calculations.

Figure 6 shows that Pd complexes with two **L2** ligands are significantly higher in energy than PdL complexes, indicating that the mono-ligated Pd dominates in this system. This is in keeping with the lack of a nonlinear effect on *ee* and the similar rates obtained using enantiopure and racemic **L2** systems.

The results of kinetic studies[17] using MPAAM ligands **L1** and **L2** are reported qualitatively in Figure 7, with detailed reaction conditions and time course curves given in the Supporting Information. For reactions using **L1** (Figure 8a), the reaction rate is positive order in concentration of the carboxylic acid substrate **1**, zero order in aryl iodide **2** concentration, and positive order in [Pd]. Interestingly, decreasing the ligand concentration from Pd:**L1** = 1:2 to Pd:**L1** = 1:1 *increases* the rate significantly (Figure 7a). Reactions using **L2** similarly showed positive order dependence on [Pd] and zero order dependence on the aryl iodide [**2**] but gave zero order dependence on both [**1**] and [**L2**] (Figure 8b). Kinetic analysis of the fluorinated ligand systems **L1-F** and **L2-F** showed enhanced rates compared to to kinetic dependences were obse

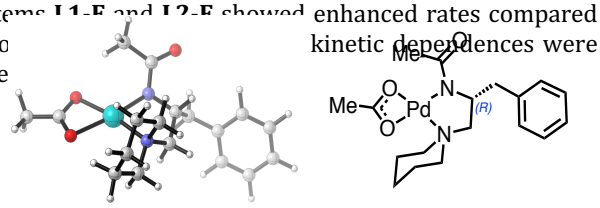

[*R*-Pd(L2)(OAc)]: ΔΔG = 0.0 kcal mol^{-1}

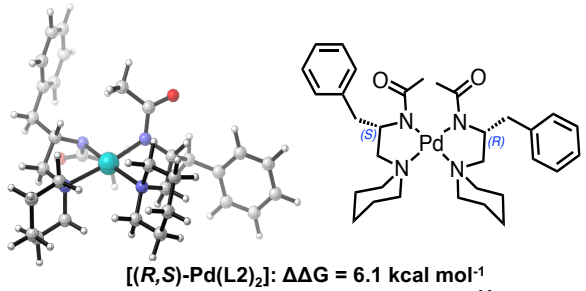

[(*R,S*)-Pd(L2)$_2$]: ΔΔG = 6.1 kcal mol^{-1}

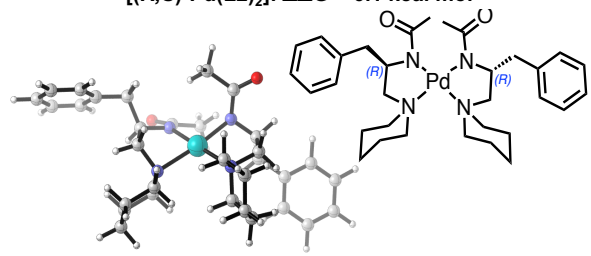

[(*R,R*)-Pd(L2)$_2$]: ΔΔG = 6.5 kcal mol^{-1}

Figure 6. Relative stabilities of lowest energy conformers of species formed from $Pd(OAc)_2$ and **L2.** [(*R*)-Pd(**L2**)$_2$] (top); [(*R,S*)-Pd(**L2**)$_2$] (middle); [(*R,R*)-Pd(**L2**)$_2$] (bottom). SMD (Generic,eps=16.7)/M06/ 6-311+G(d,p)//B3LYP/6-31G(d).

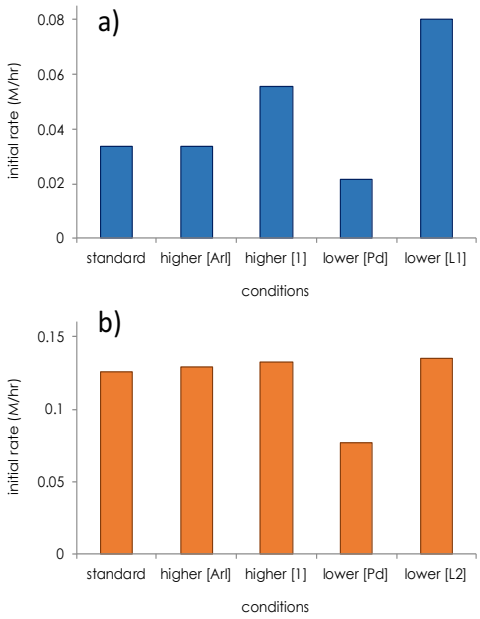

Figure 7. Kinetic studies of the reaction of Scheme 2 under the variations shown of the standard conditions given in Scheme 2. a) using **L1**; b) using **L2**. Higher [ArI] = 0.5 M; higher [**1**] = 0.3 M; lower [Pd] = 0.01 M; lower [**L1**] = 0.01 M; lower [**L2**] = 0.02 M. Time course data given in the Supporting Information.

A deuterium kinetic isotope effect of k_H/k_D = 1.6 for **L1** and 3.3 for **L2** was observed using cyclopropane-2,2,3,3-d4-carboxylic acid (see Supporting Information). Under standard conditions with Pd:L = 1:2, the reaction with **L2** proceeded nearly fourfold faster than that with **L1**. Ligand **L3** showed kinetic behavior similar to **L1**, in particular exhibiting an increase in rate with decreasing ligand concentration. All three ligand systems gave similar enantiomeric excess values between 70-80% *ee* under the conditions of these kinetic experiments, which are more dilute than those originally reported by the Yu group.

These kinetic results showing first order behavior in [Pd] support the computational and crystallographic findings that mono-Pd species acts as the active catalyst in these systems. The unusual negative dependence on [**L1**] may be rationalized in terms of the observation of a negative nonlinear effect on *ee* and the difference in reaction rate between racemic and enantiopure catalysts shown in Figure 1. Two prominent models for nonlinear effects in asymmetric catalysis[9-11] developed by Kagan and Noyori attribute the effects to the formation of higher order M(**L**)$_n$ species (where n > 1), although explanations invoking phase behavior have also been proposed in cases where incomplete dissolution of the catalyst and/or ligand occurs, which we may rule out in the present case.[18] The Kagan ML$_2$ model proposes that nonlinear effects will be observed in cases where bis-ligated species dominate the system and serve as the active catalyst.[9] Negative nonlinear effects may be observed when the heterochiral species exhibits higher activity and stability than homochiral species. In this case, the rate of reaction for racemic catalysts is predicted to be higher than that for the enantiopure ligand, which is observed in the **L1** and **L3** system. However, the instability of the calculated heterochiral bis-ligated species makes it unlikely that this model describes ligand systems **L1** and **L2**.

Noyori studied nonlinear effects in the alkylation of aldehydes by dialkylzinc complexes catalyzed by chiral amino alcohols, where monomeric species are active catalysts and dimeric species act as off-cycle spectator species.[19] A positive nonlinear effect on enantioselectivity is observed when the heterochiral dimeric complex of chiral Zn alkoxides is more stable than the homochiral complexes. In such a case, the rate for enantiopure catalysts will always be higher than that for racemic catalysts, in contrast to our observation.

The features of a further type of a negative nonlinear effect, related to the Noyori monomer-active case, occurs where equilibria between mono- and bis-ligated species exist only between homochiral species due to the instability of heterochiral bis-ligated species. Because of these equilibria, the relative concentrations of the active mono-ligated PdL$_R$ and PdL$_S$ differ from the total ligand *ee*. At lower ligand concentrations, a higher fraction of the total [Pd] is present as the active mono-ligated species compared to the bis-ligated species. For a given total L$_R$ + L$_S$ ligand concentration, the minor enantiomer of the ligand exhibits a *higher* relative concentration of active mono-ligated [Pd(**L**)(OAc)] than does the major enantiomer, resulting in a negative nonlinear effect on product *ee*. This is shown in eq 2.

$$\frac{PdL_R}{PdL_S} = \frac{L_R}{L_S} \cdot \frac{PdL_RL_R}{PdL_SL_S} \qquad (2)$$

Given these considerations and the values of K_{eq} derived from our computational models, we were able to predict the magnitude of the nonlinear effect with remarkable accuracy as shown by the dashed line in Figure 1 (top). Our observation represents a rare case of such a nonlinear effect. To the best of our knowledge, the only other report of a similar type of nonlinear effect was that observed by Hayashi and coworkers in Rh-catalyzed 1,4-addition of phenylboronic acid to enones, in which an inactive homochiral dimeric hydroxorhodium complex was observed to lie off of the catalytic cycle.[20]

The formation of off-cycle, homoleptic Pd(**L**)$_2$ species also explains the effect of ligand enantiomeric purity on rate for **L1** and **L3**. When the same absolute concentration of ligand L$_{tot}$ is divided between L$_R$ and L$_S$, the concentration of the total active PdL species (PdL$_R$ + PdL$_S$) will be greater than for the case when L$_{tot}$ is comprised of a single enantiomer of the ligand. This consideration predicts that the reaction rate should be higher for a racemic mixture of PdL$_R$ + PdL$_S$ compared with the enantiopure case. Indeed, as was shown in Figure 1b, the racemic mixture is 1.5 times faster than enantiopure ligand, in good agreement with our prediction of a relative rate of 1.7.

The dependences on substrate concentrations observed in Figure 7 implicate the steps shown in Scheme 3 as key for determining rate and enantioselectivity. Reversible

substrate binding precedes the C-H abstraction step, which is rate determining for the **L2** system and partially rate determining for **L1**. The relative populations of [Pd(**L1**)(OAc)] and [Pd(**L1**)(**1-H**)] differ for **L1** and **L2**; the higher KIE value and lower order in substrate [**1**] for **L2** suggest that the [Pd] complex rests predominantly at [Pd(**L2**)(**1-H**)], while for **L1** the catalyst is divided between [Pd(**L1**)(OAc)] and [Pd(**L1**)(**1-H**)]. All subsequent steps in the catalytic cycle, including oxidative addition of the aryl iodide, occur after the rate determining step and are kinetically invisible.

Scheme 3. Kinetically Relevant Steps in the Reaction of Scheme 2.

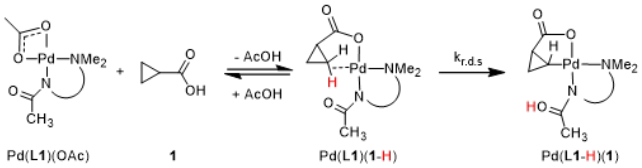

We also explored computationally the enantioselectivity in the C–H metalation-deprotonation step using substrate **1** and ligand **L1**. The optimized structures and relative free energies of the most favorable transition states for the two enantiomers are shown in Figure 8. In both transition states, the Pd(II) center is coordinated to the tertiary amine of the ligand, the N-atom of the deprotonated amide, and the carboxylate of the substrate **1**. The O-atom of the amide acts as an intramolecular base in a concerted metalation/deprotonation to activate the (sp^3)C–H bond and facilitate the Pd–C bond formation. **TS(*S*)** is more favorable than **TS(*R*)** by 4.5 kcal/mol, which overestimates the experimental selectivity but is consistent with the experimental trend for stereoselectivity.

Enantioselectivity arises from the different orientation of the amide group in the *R* and *S* transition states shown in Figure 8. There is more severe distortion of the six-membered bis-chelate of **L1** in **TS(*R*)**, where the amide group rotates into the plane of the Pd square planar complex in order to deprotonate the pro-(*R*) proton. This is shown more dramatically in Figure 9, which is an illustration of overlays of the reactant complex in red with **TS(*S*)** in blue (on the left) and with **TS(*R*)** in green (on the right). The amide group in the reactant complex is pre-organized to deprotonate the pro-(*S*) hydrogen, but in TS(*R*), distortions of the amide group and the 6-membered diazapalladacycle are required to achieve the transition state.

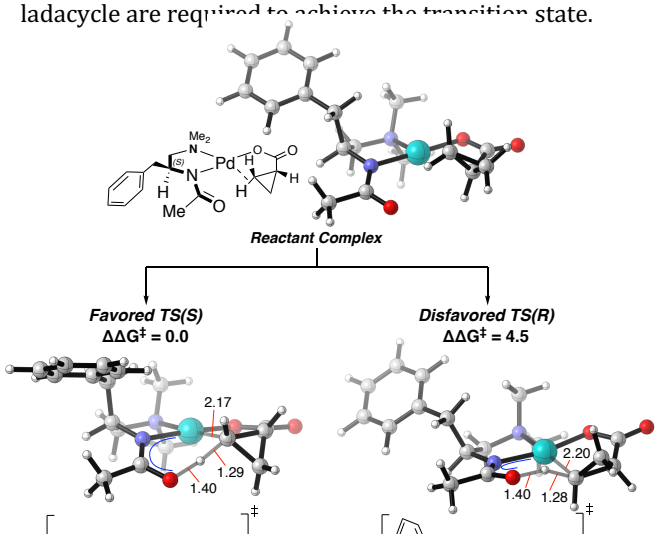

Figure 8 DFT-optimized structures and relative free energies of the two enantiomeric C–H metalation-deprotonation reactant complex and transition states.

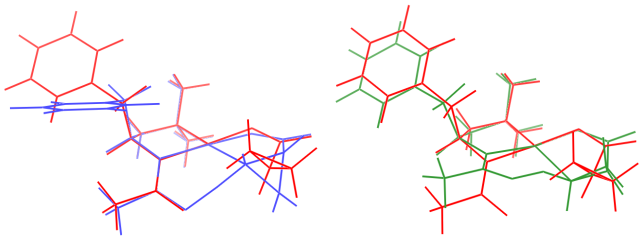

Figure 9. Overlay of reactant complex in red with TS(*S*) in blue and TS(*R*) in green.

These studies lead to the proposed catalytic mechanism shown in Scheme 4 for **L1**. Reversible substrate binding to form the reactive complex [Pd(**L1**)(OAc)-**1**] is followed by rate-determining C–H activation via the transition state shown in Figure 8. Oxidative addition of the aryl iodide is followed by reductive elimination and regeneration of the active mono-ligated catalyst PdL, which is in equilibrium with its homochiral di-ligated species in the case of **L1** and **L3**. The fraction of total Pd diverted to this off-cycle species increases with increasing ligand concentration, slowing the rate. Pd complexes with **L2**, by contrast, do not exhibit this off-cycle di-ligated species. The steps within the catalytic cycle pertain to all three ligand systems.

Scheme 4. Proposed Catalytic Cycle with Enantiopure L1.

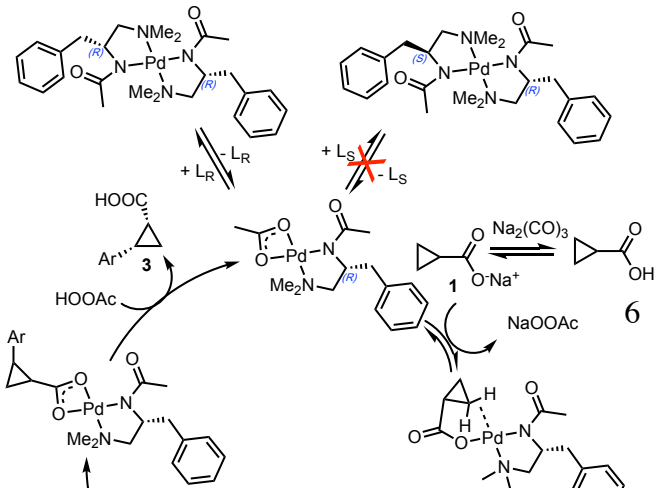

The inverse behavior of rate with ligand concentration for **L1** suggests that higher Pd:L ratios would provide optimal efficiency by effectively allowing a higher fraction of the Pd to be present as the active monoligated species. However, the robustness of the system must also be considered. For **L1**, the reaction begins to exhibit catalyst deactivation at Pd:L ratios less than 1:2, and enantioselectivity is also eroded. In the case of **L3**, excess free ligand does not adversely influence rate and may also help maintain robustness in the event of catalyst deactivation via ligand dissociation. Indeed, we found that the total turnover number could be tripled for reactions in the presence of eight equivalents of ligand **L3** (see Supporting Information).

CONCLUSIONS

In summary, the formation of off-cycle, homoleptic Pd(**L**)$_2$ species are implicated for Pd with ligands **L1** and **L3** under the standard reaction conditions outlined in Scheme 1. The formation of these species in solution was probed by NMR titrations and kinetics modeling, and the structures of several Pd(**L**)$_2$ species were determined by single-crystal X-ray diffraction. In ligand systems **L1** and **L3**, an unusual *negative* nonlinear effect on enantioselectivity, DFT calculations, and model predictions of reaction rate for the racemic compared to the enantiopure case also support a mechanistic model with the formation of stable, off-cycle, homoleptic Pd(L)$_2$ species. Additional NMR experimentation, DFT calculations, and crystallographic data not only provide support that accumulation of this species is the direct result of increased ligand-to-metal loadings, but they are also consistent with our observations of reaction rate, turnover number (TON), and product enantiomeric excess (*ee*).

We also report that the formation of these Pd(**L**)$_2$ species can be prevented by manipulating the steric parameters of the tertiary amine group in the MPAAM family of ligands. For example, these combined findings have led to the development of a new ligand in the MPAAM family, **L2**, which disfavors the formation of dimeric Pd(**L2**)$_2$ complexes. Instead, only the catalytically active, mono-substituted [Pd(**L2**)(OAc)] species is observed, allowing for a higher population of active catalyst to be present in solution and results in superior catalytic performance. The use of ligand sterics to suppress multi-ligated off-cycle species may be a general approach to achieving higher efficiency in these systems. Finally, this work demonstrates the subtle influence of ligand structure on reaction kinetics and mechanism enabling the future design of efficient enantioselective C–H functionalization catalysts.

AUTHOR INFORMATION

Corresponding Authors

K. N. Houk houk@chem.ucla.edu
John F. Berry berry@chem.wisc.edu
Jin-Quan Yu yu200@scripps.edu
Donna Blackmond blackmond@scripps.edu

§Present address: kbay@laverne.edu, Department of Chemistry, University of La Verne, 1950 Third St, La Verne, CA 91750
†Present address: erik.plata@utrgv.edu, Department of Chemistry, University of Texas Rio Grande Valley, One W. University Dr., Brownsville, TX 78520
‡Present address: The Warren and Katharine Schlinger Laboratory for Chemistry and Chemical Engineering, Division of Chemistry and Chemical Engineering, California Institute of Technology, Pasadena, California 91125 USA

ORCID
0000-0001-9829-8375 (D.G.B.)
0000-0003-3560-5774 (J.-Q.Y.)
0000-0002-6805-0640 (J.F.B.)
0000-0002-8387-5261 (K.N.H.)
0000-0002-7326-2509 (D.E.H.)

Notes

The authors declare no competing financial interest.

ACKNOWLEDGMENT

This work was supported by the National Science Foundation (USA) under the NSF Center for Selective C–H Functionalization (CHE-1700982). Computations were performed on the Hoffman2 cluster at UCLA and the Extreme Science and Engineering Discovery Environment (XSEDE), which is supported by the NSF (OCI-1053575). Dr. Jason Chen and Brittany Sanchez of the Scripps Automated Synthesis Center are acknowledged for valuable discussions and guidance on analytical methods.

ASSOCIATED CONTENT

Supporting Information available: Details of ligand synthesis, procedures for kinetic experiments, experiments on nonlinear effects, crystallization of Pd species, computational procedures.

REFERENCES

1 For selected reviews of enantioselective C–H functionalization, see: (a) Giri, R.; Shi, B.-F.; Engle, K. M.; Maugel, N.; Yu, J.-Q. Transition Metal-Catalyzed C–H Activation Reactions: Diastereoselectivity and Enantioselectivity. *Chem. Soc. Rev*. **2009**, *38*, 3242–3272. (b) Newton, C. G.; Wang, S.-G.; Oliveira, C. C.; Cramer, N. Catalytic Enantioselective Transformations Involving C–H Bond Cleavage by Transition-Metal Complexes. *Chem. Rev*. **2017**, *117*, 8908–8976. (c) Saint-Denis, T. G.; Zhu, R.-Y.; Chen, G.; Wu, Q.-F.; Yu, J.-Q. Enantioselective C(sp^3)–H Bond Activation by Chiral Transition Metal Catalysts. *Science* **2018**, *359,* eaao4798.

2 (a) Shi, B.-F.; Maugel, N.; Zhang, Y.-H.; Yu, J.-Q. Pd(II)-Catalyzed Enantioselective Activation of C(sp^2)–H and C(sp^3)–H Bonds Using Monoprotected Amino Acids as Chiral Ligands. *Angew. Chem. Int. Ed.* **2008**, *47*, 4882–4886. (b) Engle, K. M. The Mechanism of Palladium(II)-Mediated C–H Cleavage with Mono-*N*-Protected Amino Acid (MPAA) Ligands: Origins of Rate Acceleration. *Pure Appl. Chem.* **2016**, *88*, 119–138. (c) Hill, D. E.; Bay, K. L.; Yang, Y.-F.; Plata, R. E.; Takise, R.; Houk, K. N.; Yu, J.-Q.; Blackmond, D. G. A Role for Pd(IV) in Catalytic Enantioselective C-H Functionalization with Monoprotected Amino Acid Ligands Under Mild Conditions. *J. Am. Chem. Soc.* **2017**, *139*, 18500–18503. (d) Bay, K. L.; Yang, Y.-F.; Houk, K. N. Multiple Roles of Silver Salts in Palladium-Catalyzed C–H Activations. *J. Organomet. Chem.* **2018**, *864*, 19–25; (e) Haines, B.E.; Musaev, D.G. Factors Impacting the Mechanism of Mono-*N*-Protected Amino Acid Ligand-Assisted and Directing-Group-Mediated C-H Activation Catalyzed by Pd(II) Complex. *ACS. Catal.* **2015**, *5*, 830-840.

3 Wu, Q.-F.; Shen, P.-X.; He, J.; Wang, X.-B.; Zhang, F.; Shao, Q.; Zhu, R.-Y.; Mapelli, C.; Qiao, J. X.; Poss, M. A. Yu, J.-Q. Formation of α-Chiral Centers by Asymmetric β-C(sp^3)–H Arylation, Alkenylation, And Alkynylation. *Science* **2016**, *355*, 499–503. b) He, J.; Shao, Q.; Wu, Q.-F.; Yu, J.-Q. Pd(II)-Catalyzed Enantioselective C(sp^3)–H Borylation. *J. Am. Chem. Soc.* **2017**, *139*, 3344–3347

4 (a) Chen, G.; Gong, W.; Zhuang, Z.; Andrä, M. S.; Chen, Y. Q.; Hong, X.; Yang, Y.-F.; Liu, T.; Houk, K. N.; Yu, J.-Q. Ligand-Accelerated Enantioselective Methylene C(Sp^3)–H Bond Activation. *Science* **2016**, *353*, 1023–1027. (b) Hill, D. E.; Pei, Q.-L.; Zhang, E.-X.; Gage, J. R.; Yu, J.-Q.; Blackmond, D. G. A General Protocol for Addressing Speciation of the Active Catalyst Applied to Ligand-Accelerated Enantioselective C(sp^3)-H Bond Arylation. *ACS Catal.* **2018**, *8*, 1528–1531.

5 Shen, P.-X.; Hu, L.; Shao, Q.; Hong, K.; Yu, J.-Q. Pd(II)-Catalyzed Enantioselective C(sp^3)–H Arylation of Free Carboxylic Acids. *J. Am. Chem. Soc.* **2018**, *140*, 6545–6549.

6 Zhuang, Z.; Yu, J.-Q.; Pd(II)-Catalyzed Enantioselective γ-C(sp3)–H Functionalizations of Free Cyclopropylmethylamines. *J.Am. Chem. Soc.* **2020**, *142*, 12015-12019.

7 a) Gao, D.-W.; Gu, Q.; You, S.-L., Pd(II)-Catalyzed Intermolecular Direct C–H Bond Iodination: An Efficient Approach toward the Synthesis of Axially Chiral Compounds via Kinetic Resolution. *ACS Catal.* **2014,** *4*, 2741-2745; b) He, C.; Gaunt, M. J., Ligand-Enabled Catalytic C–H Arylation of Aliphatic Amines by a Four-Membered-Ring Cyclopalladation Pathway. *Angew. Chem. Int. Ed.* **2015,** *54*, 15840-15844; c) He, C.; Gaunt, M. J., Ligand-assisted palladium-catalyzed C–H alkenylation of aliphatic amines for the synthesis of functionalized pyrrolidines. *Chemical Science* **2017,** *8*, 3586-3592; d) Hong, B.; Li, C.; Wang, Z.; Chen, J.; Li, H.; Lei, X., Enantioselective Total Synthesis of (−)-Incarviatone A. *J. Am. Chem. Soc.* **2015,** *137*, 11946-11949; e) Zhang, Z.; Wang, J.; Li, J.; Yang, F.; Liu, G.; Tang, W.; He, W.; Fu, J.-J.; Shen, Y.-H.; Li, A.; Zhang, W.-D., Total Synthesis and Stereochemical Assignment of Delavatine A: Rh-Catalyzed Asymmetric Hydrogenation of Indene-Type Tetrasubstituted Olefins and Kinetic Resolution through Pd-Catalyzed Triflamide-Directed C–H Olefination. *J. Am. Chem. Soc.* **2017,** *139*, 5558-5567; f) Qi, C.; Wang, W.; Reichl, K. D.; McNeely, J.; Porco Jr., J. A., Total Synthesis of Aurofusarin: Studies on the Atropisomeric Stability of Bis-Naphthoquinones. *Angew. Chem. Int. Ed.* **2018,** *57*, 2101-2104 g) Boursalian, G. B.; Ngai, M.-Y.; Hojczyk, K. N.; Ritter, T. Pd-Catalyzed Aryl C–H Imidation with Arene as the Limiting Reagent. *J. Am. Chem. Soc.* **2013**, *135*, 13278-13281; h) Cook, A. K.; Sanford, M. S. Mechanism of the Palladium-Catalyzed Arene C–H Acetoxylation: A Comparison of Catalysts and Ligand Effects. *J. Am. Chem. Soc.* **2015**, *137*, 3109-3118; i) McNally, A.; Haffemayer, B.; Collins, B. S. L.; Gaunt, M. J. Palladium-catalysed C–H activation of aliphatic amines to give strained nitrogen heterocycles. *Nature*, **2014**, *510*, 129-133; j) Rodrigalvarez, J.; Nappi, M.; Azuma, H.; Flodén, N. J.; Burns, M. E.; Gaunt, M. J. Catalytic C(sp^3)–H Bond Activation in Tertiary Alkylamines. *Nat. Chem*. **2020**, *12*, 76–81; k) Smalley, A.; Gaunt, M. J. Mechanistic Insights into the Palladium-Catalyzed Aziridination of Aliphatic Amines by C–H Activation. *J. Am. Chem. Soc.* **2015**, *137*, 10632-10641; l) Jaworski, J. N.; Kozack, C. V.; Tereniak, S. J.; Knapp, S. M. M.; Landis, C. R.; Miller, J. T.; Stahl, S. S. Operando Spectroscopic and Kinetic Characterization of Aerobic Allylic C–H Acetoxylation Catalyzed by Pd(OAc)2/4,5-Diazafluoren-9- one. *J. Am. Chem. Soc.* **2019**, *141*, 10462-10474.

8 Zhang, Y-H.; Shi, B.-F.; Yu, J.-Q. Pd(II)-Catalyzed Olefination of Electron-Deficient Arenes Using 2,6-Dialkylpyridine Ligands.*J. Am. Chem. Soc.* **2009**, *131*, 5072-5074.

9 (a) Puchot, C.; Samuel, O.; Dunach, E.; Zhao, S.; Agami, C.; Kagan, H. B. Nonlinear Effects in Asymmetric Synthesis. Examples in Asymmetric Oxidations and Aldolization Reactions. *J. Am. Chem. Soc.* **1986**, *108*, 2353–2357. (b) Guillaneux, D.; Zhao, S.-H.; Samuel, O.; Rainford, D.; Kagan, H. B. Nonlinear Effects in Asymmetric Catalysis. *J. Am. Chem. Soc.* **1994**, *116*, 9430–9439;

0 a) Blackmond, D. G. Mathematical Models of Nonlinear Effects in Asymmetric Catalysis: New Insights Based on the Role of Reaction Rate. J. Am. Chem. Soc. 1997, 119, 12934–12939; b) Blackmond D.G. Kinetic Resolution Using Enantioimpure Catalysts: Mechanistic Considerations of Complex Rate Laws *J. Am. Chem. Soc.* **2001**, *123*, 545–553.

11 For reviews see: (a) Satyanarayana, T.; Abraham, S.; Kagan, H. B. Nonlinear Effects in Asymmetric Catalysis. Angew. Chem. Int. Ed. **2009**, 48, 456–494. (b) Blackmond, D. G. Kinetic Aspects of Nonlinear Effects in Asymmetric Catalysis. Acc. Chem. Res. **2000**, 33, 402–411; (c) Noyori, R.; Kitamura, M. Enantioselective Addition of Organometallic Reagents to Carbonyl Compounds: Chirality Transfer, Multiplication, and Amplification. Angew. Chem., Int. Ed. Engl. 1991, 30, 49.

12 (a) Sugimori, T.; Shibakawa, K.; Masuda, H.; Odani, A.; Yamauchi, O. Ternary Metal(II) Complexes With Tyrosine-Containing Dipeptides. Structures of Copper(II) and Palladium(II) Complexes Involving L-Tyrosylglycine and Stabilization of Copper(II) Complexes Due to Intramolecular Aromatic Ring Stacking.Inorg. Chem. 1993, 32, 4951. (b) Haas, K., Ehrenstorfer-Schäfers, E.-M., Polborn, K. and Beck, W. Bis(dipeptide ester–H+) Complexes of Palladium(II) – Precursors for the Formation of Cyclotetrapeptides. Eur. J. Inorg. Chem. 1999, 3, 465-469. (c) Hoffmuller, W.; Kramer, R.; Maurus, M.; Polborn, K.; Beck, W. Z. Metal Complexes with Biologically Important Ligands, CXXVIII [1]. Palladium(II) Complexes with Deprotonated Peptide Esters as N,N′-Chelate Ligands. Naturforsch. B Chem. Sci. 2000, 55, 855. (d) Romero, E. A., Chen, G.; Gembicky, M.; Jazzar, R.; Yu, J.-Q.; Bertrand, G. Understanding the Activity and Enantioselectivity of Acetyl-Protected Aminoethyl Quinoline Ligands in Palladium-Catalyzed β-C(sp3)–H Bond Arylation Reactions. J. Am. Chem. Soc. 2019, 141, 16726-16733.

13 Engle, K. M.; Mei, T.-S.; Wasa, M.; Yu, J.-Q. Weak Coordination as a Powerful Means for Developing Broadly Useful C–H Functionalization Reactions. Acc. Chem. Res. 2012, 45, 788–802.
14 See Supporting Information for more details.
15 a) Bhaskar, R.; Sharma, A.K.; Singh, A.K. Palladium(II) complexes of *N*heterocyclic carbene amidates derived from chalcogenated acetamide-functionalized 1*H*-benzimidazolium salts: recyclable catalyst for regioselective arylation of imidazoles under aerobic conditions. *Organomet.* **2018**, *37*, 2669-2681; b) Best, S.L.; Chattogadhyay, T.K.; Djuran, M.I.; Palmer, R.A.; Sadler, P.J.; Sóvágó, I.; Varnagy, K. Gold(III) and palladium(II) complexes of glycylglycyl-L-histidine: crystal structures of [Au^{III}(Gly-Gly-L-His-H_{-2}]Cl·H_2O and [Pd(Gly-Gly-L-His-H_{-2}] ·1.5H_2O and HisεNH *J. Chem. Soc. Dalton Trans.* **1997**, 2587-2596; c) Sakaguchi, S.; Yoo, K.S.; O'Neill, J.; Lee, J.H.; Stewart, T.; Jung, K.W. Chiral Palladium(II) Complexes Possessing A Tridentate *N*-Heterocyclic Carbene Amidate Alkoxide Ligand: Access to Oxygen-Bridging Dimer Structures. *Angew. Chemie Int. Ed.* **2008**, *47*, 9326-9329.
16 Yang, Y.-F.; Hong, X.; Yu, J.-Q.; Houk, K.N. Experimental-Computational Synergy for Selective Pd(II)-Catalyzed C-H Activation of Aryl and Alkyl Groups. *Acc. Chem. Res.***2017**, *50,* 2853-2860.
17 (a) Blackmond, D. G. Reaction Progress Kinetic Analysis: A Powerful Methodology for Mechanistic Studies of Complex Catalytic Reactions. Angew. Chemie Int. Ed. **2005**, 44, 4032–4320. (b) Mathew, J. S.; Klussmann, M.; Iwamura, H.; Valera, F.; Futran, A.; Emanuelsson, E. A. C.; Blackmond, D. G. Investigations of Pd-Catalyzed ArX Coupling Reactions Informed by Reaction Progress Kinetic Analysis. J. Org. Chem. **2006**, 71, 4711–4722. (c) Blackmond, D. G. Kinetic Profiling of Catalytic Organic Reactions as a Mechanistic Tool. J. Am. Chem. Soc. **2015**, 137, 10852–10866.
18 The slightly lower ee values obtained in our studies compared to Ref. 6 may be attributed to the overall lower concentrations employed in our kinetic studies, which were necessary due to substrate solubility considerations. Lower ligand concentrations may result in a larger contribution from background reaction.
19 Kitamura, M.; Suga, S.; Oka, H.; Noyori, R. Quantitative Analysis of the Chiral Amplification in the Amino Alcohol-Promoted Asymmetric Alkylation of Aldehydes with Dialkylzincs. *J. Am. Chem. Soc*. **1998**, *120*, 9800–9809.
20 Kina, A.; Iwamura, H.; Hayashi, T. A Kinetic Study on Rh/Binap-Catalyzed 1,4-Addition of Phenylboronic Acid to Enones: Negative Nonlinear Effect Caused by Predominant Homochiral Dimer Contribution. *J. Am. Chem. Soc.* **2006**, *128*, 3904-3905.

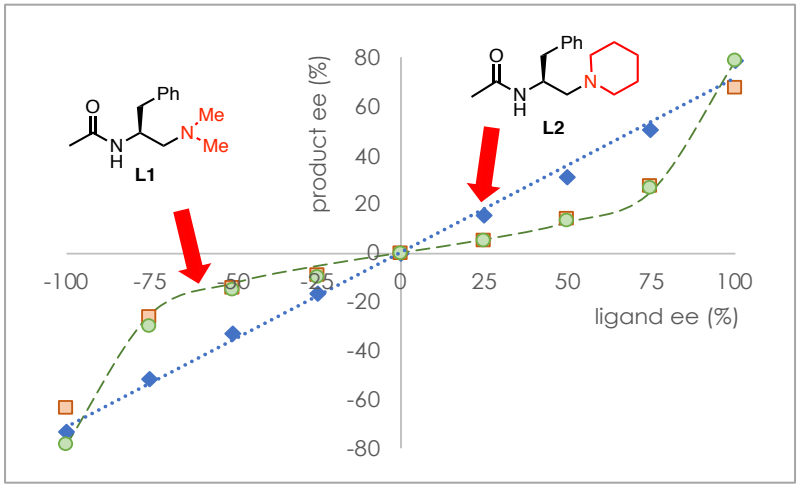
L1
L2
product ee (%)
ligand ee (%)
80
60
40
20
0
-20
-40
-60
-80
-100
-75
-50
-25
0
25
50
75
100